communications earth & environment

Article

A Nature Portfolio journal

https://doi.org/10.1038/s43247-025-02421-y

Warming and freshening coastal waters impact harmful algal bloom frequency in high latitudes

Edson Silva[1] ✉, François Counillon[1], Julien Brajard[1], Richard Davy[1], Stephen Outten[1], Lasse H. Pettersson[2] & Noel Keenlyside[1,3]

Harmful algal blooms contaminate seafood with toxins and poison humans and wildlife upon consumption. Toxic algae niches are projected to expand in high latitudes, but how the frequency of their blooms will evolve is still little known. Here we use climate models, 14 years of observations and probabilistic models of toxic algae, to assess the frequency of harmful algal blooms in a future warmer world. The warmer ocean temperatures increase the blooms in spring and autumn. However, the blooms reduce in summer as surface waters become excessively warm. Freshening reduces the blooms of species confined to high salinity ranges and has no effect on increasing the blooms. In a 3 °C warmer world, the blooms of *D. acuta* might increase by 50% and *A. tamarense* complex reduce by 40% along the Norwegian coast. Therefore, humans and wildlife are likely to become more exposed to diarrheic toxins and less to paralytic toxins.

A pressing concern in climate change is the potential increase in the frequency of harmful algal blooms (HABs) in high latitudes, where humans, shellfish farming and marine wildlife, could become much more exposed to poisoning incidents. Considering the known mechanisms of harmful algae species, a future warmer and fresher ocean with a shallower mixed layer could favour an increase in the occurrence of HABs[1,2]. The optimal environmental water conditions related to temperature, salinity, and water stratification are estimated to shift poleward and expand seasonally[3–7]. The HAB season—i.e., thermal niches, habitat suitability, or risk days—may result in more frequent HABs. However, we still have a limited understanding of the response of HABs frequency to current environmental conditions during the HAB season. Moreover, the length of the HAB season does not necessarily match the frequency of HABs. For instance, the blooms of *Alexandrium tamarense* complex (hereafter referred to as *A. tamarense*) are more frequent in the higher latitudes of Norway despite the shorter productivity season[8], while the detection frequency of their associated paralytic shellfish toxins (PST) shows no clear decreasing pattern towards the higher latitudes[9]. Those uncertainties emphasise the need for a quantitative assessment of the frequency of HABs and their evolution under climate change scenarios.

Among the many existing and known algae taxa that produce toxins and threaten humans and wildlife[9,10], *Dinophysis acuta* Ehrenberg 1839 and *A. tamarense* complex present a major risk in high latitudes. *Dinophysis* produce okadaic acid and its derivatives, the dinophysistoxins and pectenotoxins, which can have diarrheagenic effects[11,12] and are hence often referred to as diarrhetic shellfish toxins (DST). The *A. tamarense* complex comprises the species *A. catenella* (Whedon & Kofoid) Balech (Group I), *A. mediterraneum* John (Group II), *A. tamarense* (Lebour) Balech emend. John (Group III), *A. pacificum* Litaker (Group IV), and *A. australiense* Murray (Group V). Some, such as *A. catenella*, are known for producing gonyautoxins, a neurotoxin that causes paralysis and is part of the PST[1]. Both DST and PST are the most common algae toxins detected in the Scandinavian coastal waters[9]. Considering the weekly measurements of toxic algae abundance in 32 stations along the Norwegian coast, the Norwegian Food Safety Authority (NFSA) often reports *D. acuta* and *A. tamarense* HABs (when abundance exceeds 200 Cells L^{-1}) up to 3.5 and 5% of the total annual samples[13]. These toxins led to multiple poisoning incidents in the last three decades[10] and contributed to hindering the expansion of the blue mussel farming sector[14]. There is also evidence that these toxins could be related to the poisoning and death of marine mammals and seabirds[15–17]. Hence, whether harmful algae impacts will worsen in high latitudes depends largely on how the frequency of *D. acuta* and *A. tamarense* HABs evolve under climate change.

Here, we assess the frequency of *D. acuta* and *A. tamarense* blooms along the Norwegian coast for the current period and in a 3 °C warmer world. We focus on the Norwegian coast because of its diverse sub-polar and polar conditions resulting from the large latitudinal range (58–71 °N), which provides an ideal natural laboratory representing the frequency of

[1]Nansen Environmental and Remote Sensing Center, Bjerknes Centre for Climate Research, Bergen, Norway. [2]Nansen Environmental and Remote Sensing Center, Bergen, Norway. [3]Geophysical Institute, University of Bergen, Bergen, Norway. ✉e-mail: edson.silva@nersc.no

HABs in high latitudes. Additionally, we have access to a comprehensive 14-year database of harmful algae ($n = 5920$), enabling us to estimate the frequency of HABs across a range of varying environmental conditions.

Results and Discussion

Current environment and frequency of HABs

The current climatology (1995–2014) of sea surface temperature (SST), mixed layer depth (MLD), and sea surface salinity (SSS) along the Norwegian coast exhibits the typical patterns of high latitudes (Fig. 1, Supplementary Fig. 1). The ocean is warmer and has a prolonged warmer season in the south[18], although this latitudinal gradient is reduced by the northward transport of the Norwegian Atlantic current (NwAC). The southern region has the inflow of freshwater from the main rivers and the less saline waters from the Baltic Sea, which results in a notably reduced salinity and a more pronounced seasonal amplitude than the northern coast. Despite the transport of freshwater along the coast by the Norwegian Coastal current (NCC), the freshening of waters in higher latitudes is regulated mostly by short episodic inputs[19] and is less notable in climatology. Salinity is higher during the winter and decreases in the spring because of the melting of snow and the subsequent surge in freshwater inflow[19–21]. Furthermore, the

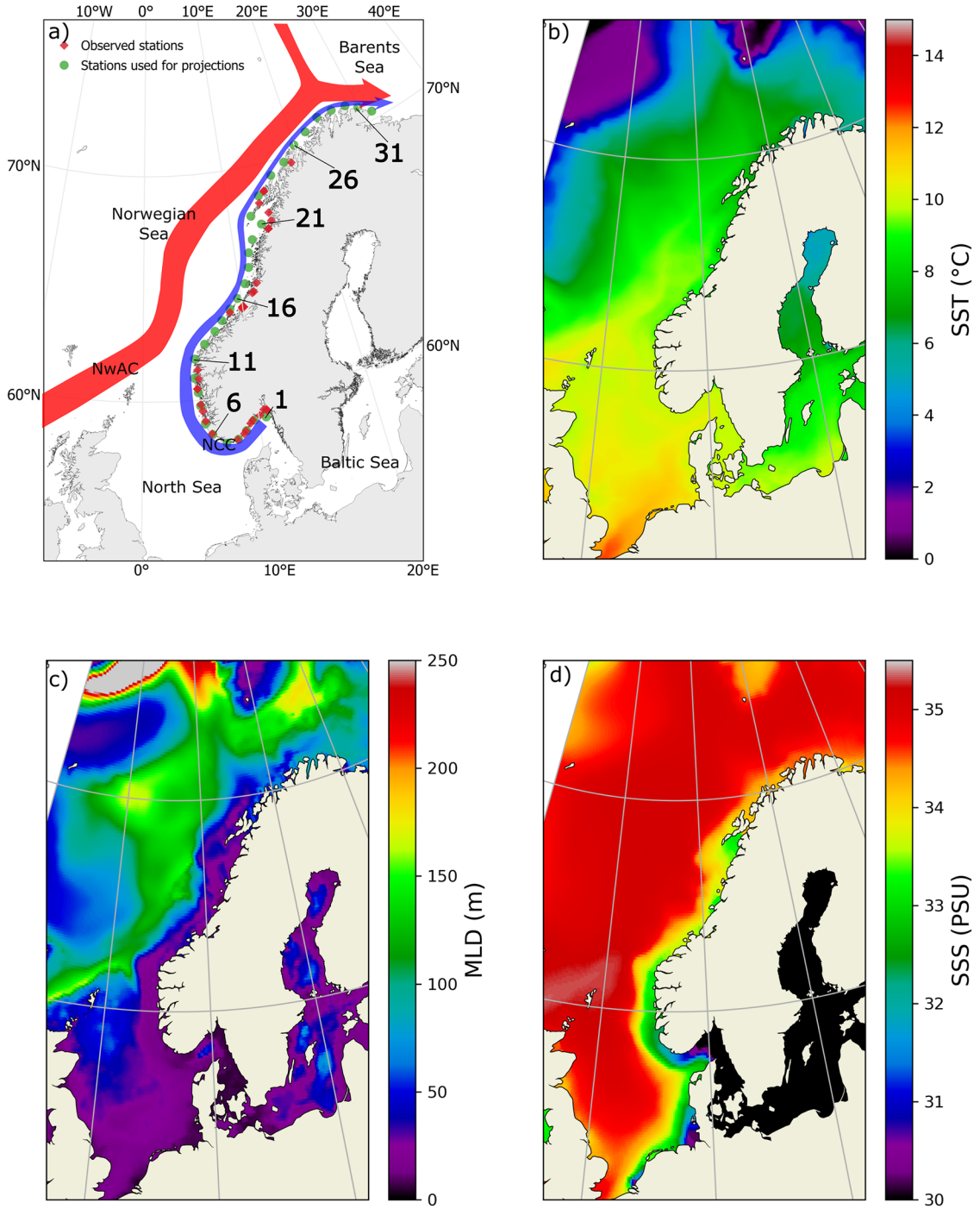

Fig. 1 | The Norwegian coastal waters. Subplot **a** exhibits a schematic view of the Norwegian coastline's main features and locations, including the NCC and NwAC, the HAB observed stations where in-situ data are available from 2006 to 2019, and the stations used for projections of the HAB frequency in future cases. Subplot **b** is the reference period (1995 – 2014) average for SST, subplot **c** is for MLD, and subplot **d** is for SSS. The seasonal time series of each station used for projections overlapping the variables in **b**–**d** are shown in Supplementary Fig. 1.

constant freshwater inflows in the southern region result in a stably stratified water column throughout the year and no seasonal pattern in MLD stratification[22]. As one moves northward, the seasonal cycle in the MLD stratification becomes apparent as the influence of river inflows and the NCC becomes less pronounced.

The HABs of both dinoflagellate species occur in relatively moderate SST (7–16 °C), with *D. acuta* blooms frequency peaking in warmer waters (14.7–16 °C) and those of *A. tamarense* in cooler conditions (9.4–11.1 °C) (Fig. 2a–c). They are rarely detected in MLD deeper than 54.3 m. A noteworthy difference between both species is that the HABs of *A. tamarense* occur only in high SSS, while the HABs of *D. acuta* occur in a wide range of SSS. Those patterns are also present in the response of the probabilistic models (Fig. 2d–g), which are further used in the projections of future HAB frequency. Moreover, the probabilistic models benefit from considering the multivariate response to all oceanographic variables. For example, the impact of SST on the frequency of *A. tamarense* HABs is only relevant in high-salinity waters, whereas, in low-salinity levels, this impact is minimal. In other words, changes in SST in the fresher southern region of Norway may be less relevant than in the high-salinity northern region. Similar responses can be observed in *D. acuta* and with the numerous possible 2d plot combinations including SST, MLD, and SSS.

The relationship between the frequency of HABs and oceanographic conditions, as well as the modelled probabilistic response, yields two important findings. Firstly, the frequency of HABs is non-linearly related to SST. While some studies acknowledge that rising SST can have adverse effects on certain toxic species[23,24], the prevailing assumption remains that warmer waters generally increase the risk of HABs. For example, the last IPCC report addressing HABs[25] only considers the enhanced growth and poleward shift of *Dinophysis* and *Alexandrium* genera, and the negative effects of rising temperature are not discussed. The non-linear relationship is sharper for *A. tamarense* but still evident for *D. acuta*. Secondly, the frequency and probability of HABs change abruptly with higher salinity. Although salinity is known as a controlling factor of algae distribution in the oceans[26–29], little is known about how it affects the frequency of HABs. The risks of both HAB species are suggested to increase in fresher waters—i.e., low salinity—due to the increased water stability and shallow MLD[1,2]. Although we exhibit the increase in probability with shallow MLD, the low SSS instead reduces the *A. tamarense* HAB risk and slightly diminishes the *D. acuta* probability.

The probabilistic response is calibrated over a large database from spring to autumn and from southern to northern Norway. Hence, the models likely reflect the biological behaviour of each species in those conditions. For example, the non-linear response to temperature and higher salinity influence was also observed in laboratory experiments. The optimal growth rates of species belonging to the *A. tamarense* complex are in mild temperatures, from 12 to 22 °C, and decrease in higher temperatures[30–36], while growth rates of *D. acuta* and *A. tamarense* increase towards 35 PSU[30–33,35,37,38]. Furthermore, complex ecosystem interactions—e.g., competition and predation[1,11,39]—and the algae life cycle may influence the models' response as well.

The optimal conditions of Mixotrophic *Dinophysis* are related to the feeding on *Mesodinium rubrum* and using their plastids to perform photosynthesis[11]. The *M. rubrum* grows better—and likely proliferates—around 24 °C and salinity 30–34 PSU[40], which could indirectly increase the probability of *D. acuta* HABs in this range. Likewise, *Dinophysis* is preyed by *Schmidingerella serrata*[41], and the SST and SSS influence on them may also impact the *D. acuta* HAB models response. Once mixotrophic *Dinophysis* spp. lacks in prey, they can rely on dissolved organic matter (DOM) to grow and continue surviving[11]. DOM aggregates at the surface due to the high phytoplankton production[42] and input of terrigenous DOM from fresh waters[43]. Shallow MLD not only facilitates the aggregation of *D. acuta* at the surface[44], but also promotes higher phytoplankton production[45,46] and likely reduce the dilution of DOM through mixing with deep waters. Those factors could explain the increase of *D. acuta* HAB probability in shallow MLD.

The complicated life history of *Alexandrium* includes haploid and diploid phases and dormancy periods through the formation of cysts[1]. *Alexandrium* blooms are mainly triggered by cyst germinations[47], which only occurs when surface and bottom temperatures—among other conditions—are within a specific range[48]. For example, the cyst germination of *A. catenella* (a toxic species in the *A. tamarense* complex) occurs from 6 to 21 °C[49], coinciding to some extent with the range of increased HAB probability. Most *Alexandrium*—and probably all—are mixotrophic[1], and temperature and salinity changes in their prey and predators likely influence the probabilistic model's response. Although these and many ecological interactions remain uncharacterised for *Alexandrium* spp., highly stratified waters are known to favour the proliferation and retention of vertically migrating *Alexandrium*[47]. This increase in proliferation is represented in the model as shown by the increase in probability in shallow MLD.

The models' responses are statistical through machine learning models and empirical by nature. The main drawback of our model is lacking a detailed explainability in the mechanistical effects leading from the models' input to the estimated probability. For example, the models estimate an increased probability of *D. acuta* HABs in relatively warmer SST without discriminating whether this is an effect on the *D. acuta* physiology or an indirect outcome through *M. rubrum*. However, the model's probability response to SST accounts implicitly for both processes. The SST influence on *D. acuta* blooms occurs via physiological responses, indirect effects through *M. rubrum*, and many other still unknown processes. The empirical modelling of HAB probability is an "averaged response" of these effects along the 14 years of observations. These responses are highly correlated with the frequency of HABs ($R > 0.8$) and can represent well their seasonal patterns[8]. By assuming the stationarity of the models' response, we can use them to assess the possible changes in the frequency of HABs in the future.

Frequency of HABs in a warmer world

We investigate the future evolution of HABs using output from three Earth system models (ESMs) under the shared socioeconomic pathway 5–8.5 (SSP585). The models are the Alfred Wegener Institute Climate Model (AWI-CM1-1-MR), the Norwegian Earth System Model (NorESM2-MM), and the Max Planck Institute for Meteorology Earth System Model (MPI-ESM1-2-HR). When the global mean surface air temperature reaches 3 °C above the 1995-2014 level, the ESMs' coastal waters become warmer and fresher with little change in the MLD (Fig. 3, Supplementary Fig. 2). However, the magnitude of these changes differs between models. Although one of the uncertainties in the evolution of HABs due to climate change is the uncertainty in climate models, we do not delve into the detailed model parameterisation that might explain these discrepancies, nor which is the most likely future. Rather, we discuss them as storylines as they span a range of plausible future conditions in the region. They serve as the basis for projecting the frequency of HABs and describing the mechanisms that can modify the HAB occurrence. The three storylines are therefore:

AWI-CM1-1-MR (warmer waters). The coastal waters become substantially warmer with a particularly high anomaly in northern Norway reaching +4.8 °C. The freshening of the coastal waters is higher than in the open ocean but still relatively low, reaching up to −0.8 PSU. Changes in the MLD are almost absent along the coast, although it shallows considerably in the open ocean. An increase in MLD up to +50 m occurs in the winter in northern Norway.

NorESM2-MM (fresher waters). The waters along the coast turn mildly warmer in southern and northern Norway, while the SST remains almost unchanged off the coast of western Norway. The seasonal patterns of SST slightly decrease by −1.2 °C in spring and increase up to 2.6 °C in summer. The freshening is substantial throughout the ocean and along the coast, where anomalies reach up to −1.5 PSU. Substantial changes in

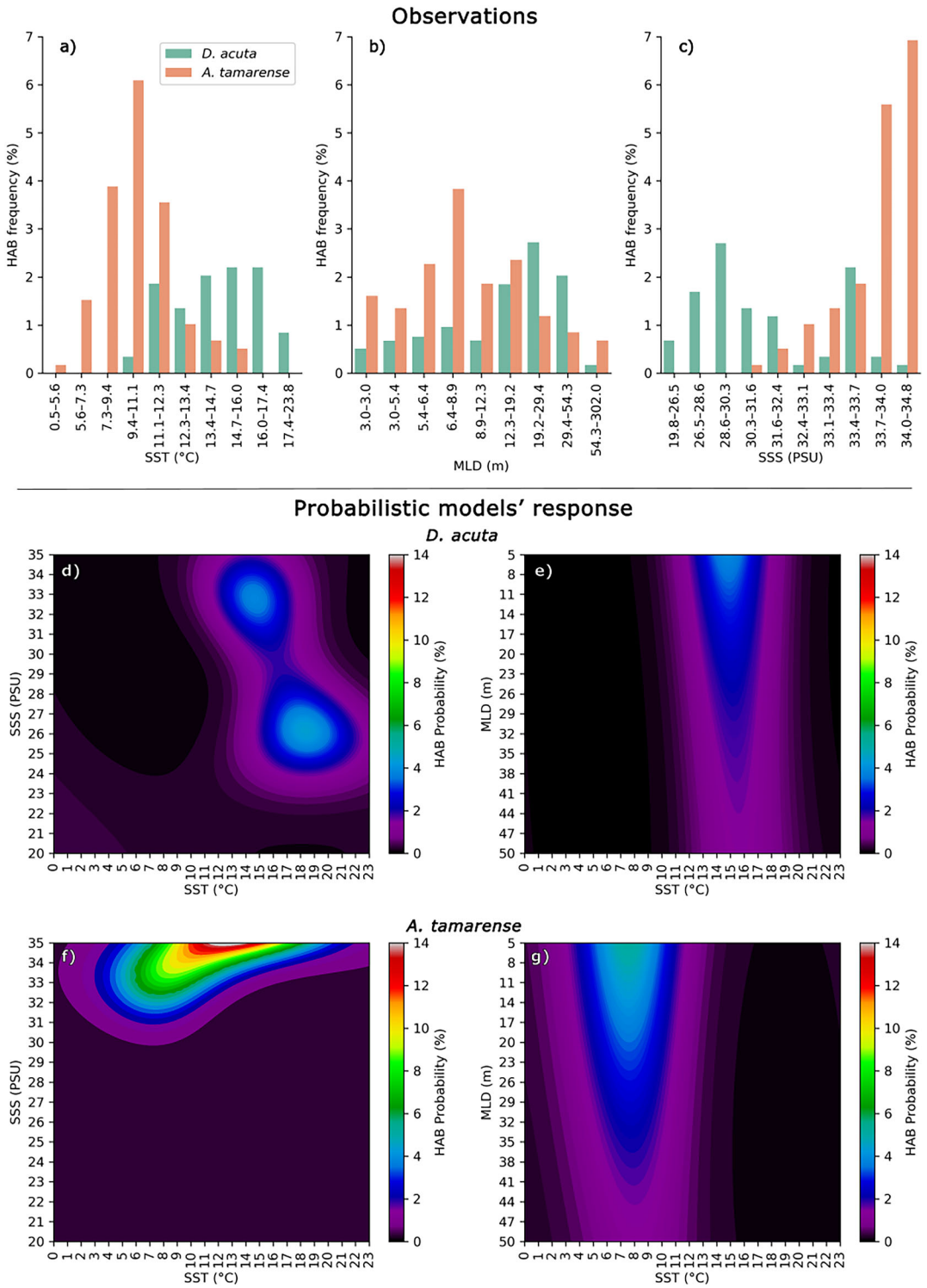

Fig. 2 | The observed frequency of HABs and HABs probabilistic models' response. Subplots **a**–**c** are the frequency of HABs (relative number of samples exceeding 200 Cells L^{-1}) for *A. tamarense* (green colour) and *D. acuta* (orange colour) observed through SST, MLD, and SSS. Observations are from 2006 to 2019 and they come from stations shown in Fig. 1a. The bin intervals are uneven to ensure each bin contains the same number of samples (592), allowing for a statistically robust estimation of the frequency. Subplots **d**–**g** are the modelled HAB probability response to SST, MLD, and for D. acuta (**d** and **e**) and *A. tamarense* (**f** and **g**). The models were developed and validated[8] using the same observed stations shown in Fig. 1a. The models' inputs are SST, MLD, SSS, and photosynthetic active radiation (PAR). PAR is not shown here (see methods section for details). The modelled response of HAB probability has four dimensions, and the 2D subplots are shown with fixed values for the remaining two hidden variables using their median, SST: 12 °C, MLD: 10 m, SSS: 32 PSU, and PAR: 30 E $m^{-2}S^{-1}$. For example, subplot d) shows the HAB probability varying in SST and SSS for a fixed value of 10 m for MLD and of 30 E $m^{-2}S^{-1}$ for PAR.

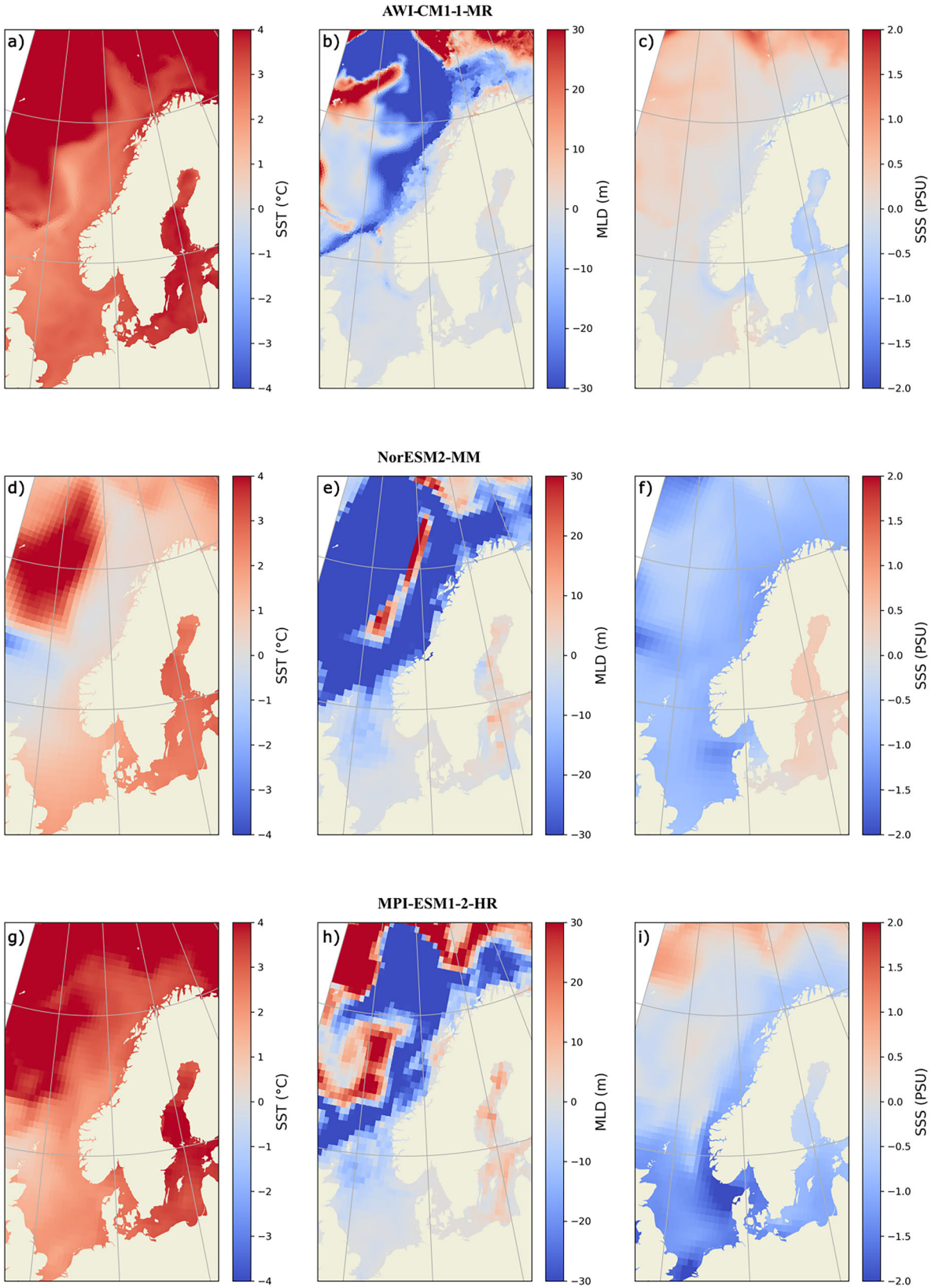

Fig. 3 | Climatology anomalies in a 3 °C warmer world. Subplots are the anomalies of SST (**a**, **d** and **g**), MLD (**b**, **e**, and **h**), and SSS (**c**, **f** and **i**) for the climate models AWI-CM1-MR (**a**, **b** and **c**), NorESM2-MM (**d**, **e** and **f**), and MPI-ESM1-2-HR (**g**, **h** and **i**). Anomalies are the 20-year average change compared to the respective models' reference period (1995–2014). The seasonal time series of each station used for projections overlapping the variables in this figure are shown in Supplementary Fig. 2.

MLD occur only in the open sea and in the Atlantic waters in northern Norway, where anomalies reach up to −70 m in spring, autumn, and winter. Changes along the rest of the coast are of minor amplitude.

MPI-ESM1-2-HR (warmer and fresher waters). The Norwegian coastal waters become considerably warmer and fresher. The SST anomalies reach up to +4.2 °C in northern Norway, and SSS reaches up to −4 PSU in southern Norway. Changes in MLD are both shallowing and deepening from autumn to spring in northern Norway, varying from −50 m to +35 m. Like the other cases, MLD remains almost unchanged along the rest of the coast.

The frequency evolution of HABs is estimated by using the probabilistic models developed by Silva et al. [8]. The models estimate the probability of each species exceeding harmful levels (> 200 CellsL^{-1}) for a given SST, MLD, and SSS, as shown in Fig. 2. The models were tuned to their probability matching the frequency of HABs, and their testing results exhibit a high correlation ($R > 0.8$) and low average bias (bias < ±1.5%). Since the models were calibrated following the NFSA monitoring system, our assessment follows a similar configuration but with some small adjustments. We use 32 stations for projections (Shown as green dots in Fig. 1a) instead of the observed stations (Shown as red dots in Fig. 1a) to evenly spread the probability estimations along the coast. The estimations are weekly and from March to November, as algae are not sampled during the winter. Given that the probability is well related to the frequency when following this setting ($n = 40$ weeks × 32 stations = 1280), the estimated probability represents the frequency of HABs.

The annual number of HABs during the reference observational period (1995–2014) is 17 for *D. acuta* and 44 for *A. tamarense* (Fig. 4a, b). The blooms of *D. acuta* are more likely – and more frequent – to occur in late summer and autumn (Fig. 4c). The highest probability is in western Norway and decreases towards the south and north due to the lower SSS and lower SST, respectively. The probability of *A. tamarense* blooms is low and limited to spring in southern Norway (Fig. 4g). Moving northwards, the cooler and higher SSS waters increase the probability and expand the season of *A. tamarense* blooms. In a future warmer world (1–3 °C), the annual number of HABs evolves differently depending on the storyline and species. The AWI-CM1-1-MR (warmer case) predicts an increase in *D. acuta* and *A. tamarense* blooms, which are driven by an increase in probability towards spring and autumn and also in summer at high latitudes for *D. acuta* (Fig. 4d and h). The NorESM2-MM (fresher case) predicts no changes in the blooms of *D. acuta* and a decrease in the blooms of *A. tamarense*. The decrease results from a substantial reduction in the probability of blooms along the coast during the main bloom season (Fig. 4e and i). The MPI-ESM1-2-HR (warmer and fresher case) predicts an increase in the blooms of *D. acuta* and a decrease in the blooms of *A. tamarense*. The probability of *D. acuta* blooms increases in spring and autumn and in summer at higher latitudes, and the probability of *A. tamarense* blooms decreases during its main season (Fig. 4f and j).

The impact of changing ocean conditions in future HABs

Given the high seasonal variability of SST in the high latitudes, the main concern has been on the seasonal expansion of optimal temperatures that allows harmful algae to grow[7,50]. Longer seasons may lead to more HABs each year as harmful algae will have more opportunities to grow and reach hazardous levels[25]. However, warmer temperatures can also negatively affect toxic algae associated with colder temperatures[24] and slightly reduce the number of risk days[5]. Our results demonstrate that the warmer ocean can increase the probability of *D. acuta* and *A. tamarense* blooms in spring and autumn, leading to an overall annual increase in the frequency of HABs. Nonetheless, a warmer ocean in summer counteracts and reduces the probability of blooms in that season, thereby mitigating the increase in their annual frequency caused by seasonal expansion. This response is evident in the warmer storylines AWI-CM1-1-MR and MPI-ESM1-2-HR for *D. acuta* and AWI-CM1-1-MR for *A. tamarense*. The relatively colder spring becomes optimal in the range associated with the increased probability of HABs, while the summer becomes excessively warm in the range with reduced probability. Thus, the SST in warmer storylines in $a + 3$ °C warmer world increases by 50% the annual frequency of *D. acuta* blooms, while it increases only by 5%—at maximum—the annual frequency of those of *A. tamarense*.

Salinity is a controlling factor in the distribution of algae in coastal waters[26–29] as they present varying physiological responses[51], including those belonging to harmful species[30–33,35,37,38]. In high latitudes, the river inflow and precipitation are likely to increase, and their seasonal patterns be altered by changes in the snowfall[22,52–54]. Consequently, salinity might be an important climate driver in the frequency of HABs. For example, the *Alexandrium* genus thrives in a wide range of salinity, and fresher coastal waters could give them competitive advantages and lead to increased frequency of HAB[1]. Nevertheless, we have lacked climate studies demonstrating the role of salinity in modulating HABs. Moreover, we are still uncertain whether freshening could favour harmful species, as non-harmful algae can also thrive in a wide range of salinity[24]. Here, we reveal the potential role of salinity in changing the frequency of HABs. The probability of *D. acuta* HABs varies marginally across the SSS levels and therefore remains unchanged in the fresher cases of NorESM2-MM and presents no reduction driven by SSS in MPI-ESM1-2-HR. In contrast, the probability of *A. tamarense* HABs varies sharply along the SSS levels and is elevated in high salinity. As a result, the frequency of *A. tamarense* HABs reduces by 40% in the fresher storyline compared to the reference period. In other words, if changes in the hydrological cycle lead to substantial freshening of the coastal waters, harmful species related to high salinity waters will likely decrease in high latitudes.

A shallow MLD—or stably-stratified waters—strengthens the pycnocline and acts as a focal point for the development of HABs[24], including dinoflagellates and the species belonging to the *Dinophysis* spp. and *Alexandrium* spp[1,11]. With increasing SST and freshening of the coastal waters in future warmer scenarios, the MLD could start to shallow earlier and increase the number of HABs. However, this earlier shallowing is relatively weak along the coast despite the pronounced warming or freshening, and is only meaningful in the open and deep ocean (Fig. 1; Supplementary Fig. 2). Possible explanations are that either the MLD is already well stratified throughout the year and hence will not become shallower, or the turbulence variability on the shelf areas reduces the expected changes[22]. Furthermore, even at a few stations where anomalies reach around −70 m (e.g., station 30 in NorESM2-MM), the MLD is still deeper than 100 m and contributes little to changing the probability of HABs. To better confirm the weak influence of MLD in a future scenario, we have tested each storyline by fixing the SST and SSS to their reference (1995–2014) and using only the MLD anomalies (+3 °C) in the HAB probabilistic models (Supplementary Fig. 3). We have not observed any substantial changes in the probability of HABs and annual frequency. Therefore, future changes in the frequency of HABs driven by MLD are likely negligible if the MLD evolves as the three climate projections presented here.

Methods

Current oceanographic observations

The current observations of SST, MLD, SSS, and photosynthetically active radiation (PAR) correspond to satellite observations and model reanalysis—hereafter referred to only as observations (Table 1). Those are the same products used for calibrating the HAB probabilistic models[8]. The PAR is not discussed in this study, but is necessary for using the HAB probabilistic models. The SST (°C) is from the European Space Agency (ESA) SST Climate Change Initiative (CCI) and the Copernicus Climate Change Service (C3S) global SST reprocessed product level 4, available in the Copernicus Marine Environment Monitoring Service (CMEMS). The product is derived by employing the Operational SST and Sea Ice Analysis System[55] that combines remote sensing and in-situ observations to produce gap-free daily average SST at 0.05 ° of spatial resolution[56]. The MLD (m) and SSS (PSU) estimations are from the CMEMS Arctic Monitoring and Forecasting Centre TOPAZ modelling system[57,58] that uses a coupled ocean–sea ice

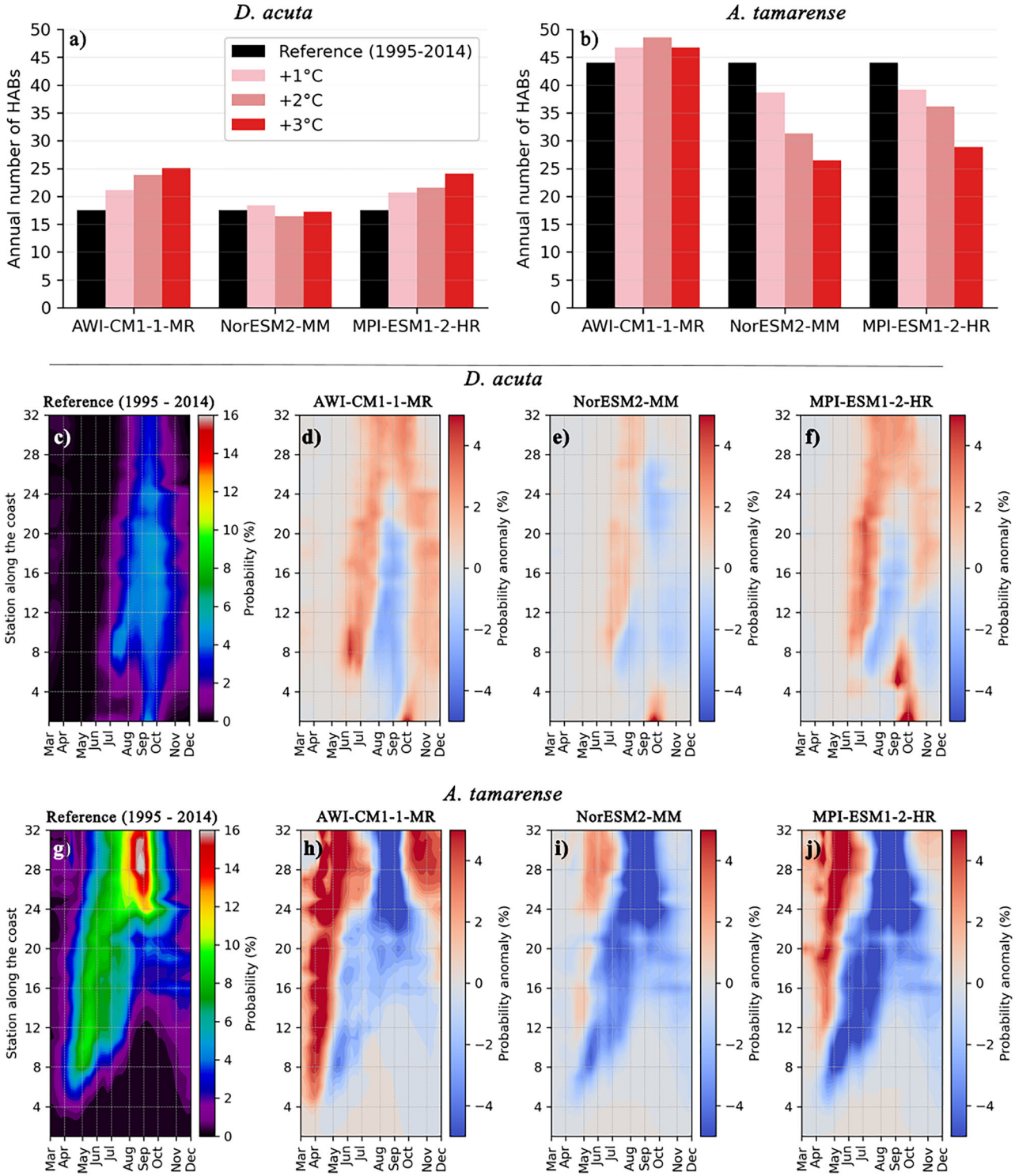

Fig. 4 | The annual number of HABs and HAB probability under the reference period and future warming levels. The annual number of HABs for **a** *D. acuta* and **b** *A. tamarense* corresponds to the average probability in **c**–**j** multiplied by the total number of samples (40 weeks × 32 stations). The seasonal HAB probability along the1 projected stations (shown in Fig. 1a) during the reference period are shown for **c** *D. acuta* and **g** *A. tamarense*. The HAB probability anomalies for a +3 °C warmer world for each species are shown for AWI-CM1-1-MR (**d** and **h**), NorESM2-MM (**e** and **i**), and MPI-ESM1-2-HR (**f** and **j**). To illustrate, the annual number of HABs of *D. acuta* shown in the reference period in **a** is the average of the probability shown in **c** multiplied by 1280 (weeks × stations), and the +3 °C numbers in **a** for each model corresponds to the changes caused by the probability anomalies in **d**–**f**.

model and weekly data assimilation for the North Atlantic and Arctic Oceans. MLD corresponds to the density criterion with a 0.01 kg m^{-3} and SSS is extracted from the surface layer. PAR (E m^{-2}d^{-1}) is retrieved using the Frouin et al. algorithm[59] and accessed from the GlobColour project that combines several satellite sensors (MODIS, SeaWiFS, and VIIRS) binned at an 8-day interval and a 4 km spatial resolution. For applying the HAB probabilistic models, we need to align the grids and standardise the time-frequency of all observations. Thus, we have reprojected all observations to

Table 1 | Summary of the observations and climate models used

Observations and climate models	Variable	Spatial resolution	Time step	Period
ESA CCI and C3S	SST	0.05 °	Daily	1995–2014
TOPAZ	MLD and SSS	12.5 km	Daily	1995–2014
GlobColour	PAR	4 km	8 Days mean	2000–2019
AWI-CM1-1-MR	SST, SSS, and MLD	8–80 km	Daily	1995–2014 2068–2087
NorESM2-MM	SST, SSS, and MLD	1 °	Daily	1995–2014 2074–2093
MPI-ESM1-2-HR	SST, SSS, and MLD	40 km	Daily	1995–2014 2077–2096

Future periods in the climate models correspond to when the global average of the Earth's surface air temperature reaches 3 °C warmer than the 1995–2014 period.

4 km spatial resolution using the nearest neighbour interpolation method and resampled the time series to weekly intervals.

Climate projections

The historical and shared socioeconomic pathway 5–8.5 (SSP585) projection of the AWI-CM1-1-MR, NorESM2-MM, and MPI-ESM1-2-HR, are used for assessing the changes in SST, MLD, and SSS (Table 1). The data were obtained from the Coupled Model Intercomparison Project (CMIP) Phase 6 (CMIP6) on the Earth System Grid Federation (ESGF) web portal nodes (https://pcmdi.llnl.gov/CMIP6/), such as the DKRZ node (https://esgf-data.dkrz.de/projects/cmip6-dkrz/). The models span well the diversity of ESMs contributing to the Coordinated Model Intercomparison Project. Two of the systems are high-resolution models (AWI-CM1 1-MR and MPI-ESM1-2-HR) and they use different model components and coordinate systems. The ocean components in MPI-ESM1-2-HR use a regular grid horizontally and vertically (geopotential depth). The AWI-CM1-1-MR uses an unstructured grid that increases the resolution in high latitudes and coastal regions. The NorESM2-MM uses an isopycnal coordinates in the vertical. The systems also have different sensitivity to anthropogenic forcing, showing a different temperature anomaly in the recent period compared to the pre-industrial period; with NorESM2-MM being on the lower side, MPI-ESM1-2-HR being medium and AWI-CM1-1-MR being on the higher side[60]. To align the models' grid with the observations, the models were also reprojected to the same grid using the nearest neighbour interpolation method and resampled to weekly time steps.

The global average of atmospheric surface temperature is estimated from 1995 to 2014 (the end of the historical period in the CMIP6 dataset) and used as a reference climatology. The Earth's surface air temperature is computed by a 20-year moving window average. There is a very large uncertainty in the future scenario, in the internal variability of the models and their climate sensitivity. IPCC recommend using a warming level that mitigates this and provides a fairer comparison. We thus assess the expected change at different warming levels (e.g., 1,2 and 3 °C), which is defined when this moving window average reaches the respective threshold. The 3 °C is reached in 2078 for AWI-CM1-1-MR, 2084 for NorESM2-MM, and 2087 for MPI-ESM1-2-HR. The seasonal averages of SST, MLD, and SSS, spanning the 20-year window, are computed for the reference seasonal climatology and the 3 °C warmer world.

Since the HAB observations and HAB frequency models are related to the observations instead of the climate models, we extract the climate change signal (anomalies) and add them to the observations corresponding to the same period. We use the delta change method as it better preserves the average amplitude of the signal[61], which we chose as the most important feature for assessing the evolution of the HAB frequency. Then, for the SST and SSS, we employ:

$$x_{obs.,3^\circ C,week} = x_{obs.,1995-2014,week} + (x_{mod.,3^\circ C,\mathrm{week}} - x_{mod.,1995-2014,week}) \quad (1)$$

where x represents SST or SSS, $x_{obs.,3^\circ C,week}$ is the variable in the 3 °C warmer world when the anomalies of the models are added to the observations reference climatology for a respective week of the year, $x_{\mathrm{mod.},3^\circ C,\mathrm{week}}$ is the projected variable of the climate model in the 3 °C warmer world, and $x_{\mathrm{mod.},1995-2014,week}$ is the climate model reference climatology. Since MLD tends to 0, we employ a relative correction that is also commonly used for precipitation[61]:

$$MLD_{obs.,3^\circ C,week} = MLD_{obs.,1995-2014,week} \times \left(\frac{MLD_{mod.,3^\circ C,week}}{MLD_{mod.,1995-2014,week}}\right) \quad (2)$$

where $MLD_{obs.,3^\circ C,week}$ is the MLD in the 3 °C warmer world when the relative anomalies of the climate models are multiplied by the observations reference climatology for a respective week of the year, $MLD_{\mathrm{mod.},3^\circ C,\mathrm{week}}$ is the projected MLD of the climate model in the 3 °C warmer world, and $MLD_{\mathrm{mod.},1995-2014,week}$ is the MLD climate model reference climatology.

HABs probability and annual frequency

The observations of HABs are samples collected weekly at a depth of 0–3 m along the coast from 2006 to 2019 where blue mussel (*Mytilus edulis*) farms operate. The data are from the regional monitoring of toxic algae and toxins conducted by the NFSA, comprising around 32 sampling sites every year. The data covers from week of the year 9 (February) to 48 (November) as HABs are unlikely to happen during the dark and cold winter season. Here, sites in the inner fjords and narrow areas are excluded because the observations and climate models' spatial resolution are too coarse to reach these regions. Therefore, the number of samples available from the analysis is reduced from an expected of 17,920 ($40 \times 32 \times 14$) to 5920. Since algae species are identified and counted by using microscopes, the current five species belonging to the *A. tamarense* complex[1] cannot be distinguished, and therefore the current assessment refers to the whole complex. We define HABs as occurrences where *D. acuta* and *A. tamarense* exceed 200 Cells L^{-1}, a threshold established by the NFSA to regulate blue mussel farming and issue public health advisories against mussel consumption.

We estimate the frequency distribution of HABs (Fig. 2a–c) by matching the in-situ algae observations with the SST, MLD, and SSS. For the probability of HABs, we use the recently developed HAB probabilistic models for the Norwegian coast[8], which were built using the same samples in this study. The models' inputs are the SST, MLD, SSS, and PAR. More details in the HAB frequency models, including training and validation, are found in the original study[8]. The probability of HABs has four dimensions that correspond to the number of inputs, and we hold two of the variables constant at their median values to show them two dimensions. In this case, the SST median is 12 °C, MLD is 10 m, SSS is 32 PSU, and PAR is 30 E $m^{-2}s^{-1}$. For example, the probability of HABs across SST and SSS 2-D plots are for an MLD fixed at 10 m and PAR at 30 E $m^{-2}s^{-1}$.

The probability of HABs for the reference period and the future warmer scenario is estimated by using the HAB probabilistic models of both species. For the reference period, the SST, MLD, and SSS inputs are from 1995 to 2014 but PAR is from 2000 to 2019. The PAR reference period is later than the others because high-quality satellite observations used for estimating PAR were not available before 2000. This shift has minimal impact as we have not observed PAR trends from 2000 to 2019 and climate projections show no PAR changes in the ice-free zones in the Nordic seas[62]. We will therefore assume that there is no change in PAR in the future climate. For the warmer world scenarios, we use the 20-year anomalies that

were added or multiplied to the observations ($x_{obs.,3\,°C,week}$). The probability of HABs is estimated for each week ($n = 40$) and station ($n = 32$) and the annual frequency of HABs corresponds to the average probability times the number of samples ($n = 40 \times 32 = 1280$).

An important assumption for the projections of HAB probability and annual frequency is that the response observed from 2006 to 2019 applies to the reference period 1995–2014 and will continue to apply when Earth's surface air temperature reaches the average of 3 °C warmer threshold. This means that the physiological response of each taxon to the input variables (e.g., SST) as well as indirect effects through non-observed processes[1,11,39]—e.g., prey-predator interactions—is assumed to remain stationary. Furthermore, we also assume that the response remains when shifting the observed stations to the stations used for the projections (see Fig. 1a). Since shellfish farms changed their location from 2006 to 2019 and the sampling stations followed them, many sampling stations are relatively close although they cover different years. Therefore, we use the stations shown in Fig. 1a to project the probability of HABs on evenly spread and well-distributed stations along the Norwegian coast.

Reporting summary

Further information on research design is available in the Nature Portfolio Reporting Summary linked to this article.

Data availability

All data analysed in this study are available in public repositories. This study has been conducted using E.U. Copernicus Marine Service Information; https://doi.org/10.48670/moi-00169 and https://doi.org/10.48670/moi-00007. GlobColour data (https://hermes.acri.fr) used in this study has been developed, validated, and distributed by ACRI-ST, France. Climate projections used in this study are AWI-CM1-MR[63] (https://doi.org/10.22033/ESGF/CMIP6.359), MPI-ESM1-2-HR[64] (https://doi.org/10.22033/ESGF/CMIP6.762), and NorESM2-MM[65] (https://doi.org/10.22033/ESGF/CMIP6.506). Observations of HABs are available at https://doi.org/10.5281/zenodo.10958487.

Code availability

HAB probabilistic models are available at https://doi.org/10.5281/zenodo.10958487.

Received: 14 November 2024; Accepted: 27 May 2025;
Published online: 09 June 2025

References

1. Klemm, K. et al. Apparent biogeographical trends in Alexandrium blooms for northern Europe: identifying links to climate change and effective adaptive actions. *Harmful Algae* **119**, 102335 (2022).
2. Wells, M. L. et al. Harmful algal blooms and climate change: learning from the past and present to forecast the future. *Harmful Algae* **49**, 68–93 (2015).
3. Townhill, B. L. et al. Harmful algal blooms and climate change: exploring future distribution changes. *ICES J. Marine Sci.***75**, 1882–1893 (2018).
4. Glibert, P. M. et al. Vulnerability of coastal ecosystems to changes in harmful algal bloom distribution in response to climate change: projections based on model analysis. *Glob. Chang. Biol.* **20**, 3845–3858 (2014).
5. Boivin-Rioux, A. et al. Predicting the effects of climate change on the occurrence of the toxic dinoflagellate Alexandrium catenella Along Canada's East coast. *Front Mar Sci* **7**, 1–20 (2021).
6. Boivin-Rioux, A. et al. Harmful algae and climate change on the Canadian East coast: exploring occurrence predictions of Dinophysis acuminata, D. norvegica, and Pseudo-nitzschia seriata. *Harmful Algae* **112**, 102183 (2022).
7. Gobler, C. J. et al. Ocean warming since 1982 has expanded the niche of toxic algal blooms in the North Atlantic and North Pacific oceans. *Proc. Natl. Acad. Sci. USA* **114**, 4975–4980 (2017).
8. Silva, E., Brajard, J., Counillon, F., Pettersson, L. H. & Naustvoll, L. Probabilistic models for harmful algae: application to the Norwegian coast. *Environ. Data Sci.* **3**, 102781 (2024).
9. Karlson, B. et al. Harmful algal blooms and their effects in coastal seas of Northern Europe. *Harmful Algae* **102**, 101989 (2021).
10. Pettersson, L. H. & Pozdnyakov, D. *Monitoring of Harmful Algal Blooms* (Springer, 2013).
11. Reguera, B., Velo-Suárez, L., Raine, R. & Park, M. G. Harmful dinophysis species: a review. *Harmful Algae* **14**, 87–106 (2012).
12. Yasumoto, T. et al. Diarrhetic shellfish toxins. *Tetrahedron* **41**, 1019–1025 (1985).
13. Silva, E. *Prediction of Harmful Algae Blooms Impacting Shellfish Farms in Norway* (Universitet i Bergen, 2023).
14. Ytrøy, E. H. *Blue Mussel Farming-a Comparison of the Norwegian and the Canadian Industries* (University of Tromsø, 2008).
15. Lefebvre, K. A. et al. Prevalence of algal toxins in Alaskan marine mammals foraging in a changing arctic and subarctic environment. *Harmful Algae* **55**, 13–24 (2016).
16. Van Hemert, C. et al. Algal toxins in Alaskan seabirds: evaluating the role of saxitoxin and domoic acid in a large-scale die-off of Common Murres. *Harmful Algae* **92**, 101930 (2020).
17. Jensen, S.-K. Are toxins from harmful algae a factor involved in the decline of harbour seal populations in Scotland? (University of St Andrews, 2015).
18. Jakowczyk, M. & Stramska, M. Spatial and temporal variability of satellite-derived sea surface temperature in the Barents Sea. *Int. J. Remote Sens.* **35**, 6545–6560 (2014).
19. Frigstad, H. et al. Influence of riverine input on Norwegian coastal systems. *Front. Mar. Sci.* **7**, 332 (2020).
20. Dankers, R. & Christensen, O. B. Climate change impact on snow coverage, evaporation and river discharge in the Sub-Arctic Tana Basin, Northern Fennoscandia. *Clim. Change* **69**, 367–392 (2005).
21. Dankers, R. & Middelkoop, H. River discharge and freshwater runoff to the Barents Sea under present and future climate conditions. *Clim. Change* **87**, 131–153 (2008).
22. Holt, J., Wakelin, S., Lowe, J. & Tinker, J. The potential impacts of climate change on the hydrography of the northwest European continental shelf. *Prog. Oceanogr.* **86**, 361–379 (2010).
23. Hallegraeff, G. M. Ocean climate change, phytoplankton community responses, and harmful algal blooms: a formidable predictive challenge. *J. Phycol.* **46**, 220–235 (2010).
24. Yan, Z., Kamanmalek, S., Alamdari, N. & Nikoo, M. R. Comprehensive insights into harmful algal blooms: a review of chemical, physical, biological, and climatological influencers with predictive modeling approaches. *J. Environ. Eng.* **150**, 03124002 (2024).
25. Intergovernmental Panel on Climate Change (IPCC). Changing ocean, marine ecosystems, and dependent communities. In *Proc.The Ocean and Cryosphere in a Changing Climate* 447–588 (Cambridge University Press, 2022).
26. Gasinaite, Z. R. et al. Seasonality of coastal phytoplankton in the Baltic Sea: influence of salinity and eutrophication. *Estuar Coast Shelf Sci.* **65**, 239–252 (2005).
27. Stefanidou, N., Genitsaris, S., Lopez-Bautista, J., Sommer, U. & Moustaka-Gouni, M. Unicellular eukaryotic community response to temperature and salinity variation in mesocosm experiments. *Front. Microbiol.* **9**, 2444 (2018).
28. Hernando, M., Varela, D. E., Malanga, G., Almandoz, G. O. & Schloss, I. R. Effects of climate-induced changes in temperature and salinity on phytoplankton physiology and stress responses in coastal Antarctica. *J. Exp. Mar. Biol. Ecol.* **530**, 531 (2020).

29. Olli, K., Ptacnik, R., Klais, R. & Tamminen, T. Phytoplankton species richness along coastal and estuarine salinity continua. *Am. Nat.* **194**, 703657 (2019).
30. Persich, G. & Garcia, V. Influência da temperatura, salinidade e luz sobre o crescimento do dinoflagelado Alexandrium tamarense (dinoflagellata, dinophyceae) da plataforma continental adjacente ao estuário da lagoa dos patos. *Atlântica* **32**, 25–37 (2011).
31. Lee, C., Lee, O. & Lee, S. Impacts of temperature, salinity and irradiance on the growth of ten harmful algal bloom-forming microalgae isolated in Korean coastal waters. *Sea J. Kor. Soc. Oceanogr.***10**, 79–91 (2005).
32. Bill, B. D., Moore, S. K., Hay, L. R., Anderson, D. M. & Trainer, V. L. Effects of temperature and salinity on the growth of Alexandrium (Dinophyceae) isolates from the Salish Sea. *J. Phycol.* **52**, 230–238 (2016).
33. Paredes-Mella, J., Varela, D., Fernández, P. & Espinoza-González, O. Growth performance of Alexandrium catenella from the Chilean fjords under different environmental drivers: plasticity as a response to a highly variable environment. *J. Plankton Res.* **42**, 119–134 (2020).
34. Navarro, J. M., Muñoz, M. G. & Contreras, A. M. Temperature as a factor regulating growth and toxin content in the dinoflagellate Alexandrium catenella. *Harmful Algae* **5**, 762–769 (2006).
35. Etheridge, S. M. & Roesler, C. S. Effects of temperature, irradiance, and salinity on photosynthesis, growth rates, total toxicity, and toxin composition for Alexandrium fundyense isolates from the Gulf of Maine and Bay of Fundy. *Deep Sea Res. Part II: Top. Stud. Oceanogr.* **52**, 2491–2500 (2005).
36. Eckford-Soper, L. K., Bresnan, E., Lacaze, J. P., Green, D. H. & Davidson, K. The competitive dynamics of toxic Alexandrium fundyense and non-toxic Alexandrium tamarense: the role of temperature. *Harmful Algae* **53**, 135–144 (2016).
37. Parkhill, J. Effects of salinity, light and inorganic nitrogen on growth and toxigenicity of the marine dinoflagellate Alexandrium tamarense from northeastern Canada. *J. Plankton Res.* **21**, 939–955 (1999).
38. Rial, P. et al. Interaction between temperature and salinity stress on the physiology of Dinophysis spp. and Alexandrium minutum: implications for niche range and blooming patterns. *Aquat. Microb. Ecol.***89**, 1–22 (2023).
39. Reguera, B. et al. Dinophysis, a highly specialized mixoplanktonic protist. *Front. Protistol.* **1**, 1328026 (2024).
40. Fiorendino, J. M., Smith, J. L. & Campbell, L. Growth response of dinophysis, mesodinium, and teleaulax cultures to temperature, irradiance, and salinity. *Harmful Algae* **98**, 101896 (2020).
41. Maneiro, I. et al. Zooplankton as a potential vector of diarrhetic shellfish poisoning toxins through the food web. *Mar. Ecol. Prog. Ser.* **201**, 155–163 (2000).
42. Digernes, M. G. et al. Contrasting seasonal patterns in particle aggregation and dissolved organic matter transformation in a sub-Arctic fjord. *Biogeosciences* **22**, 601–623 (2025).
43. Benner, R., Louchouarn, P. & Amon, R. M. W. Terrigenous dissolved organic matter in the Arctic Ocean and its transport to surface and deep waters of the North Atlantic. *Glob. Biogeochem. Cycles* **19**, 1–11 (2005).
44. Lindahl, O., Lundve, B. & Johansen, M. Toxicity of Dinophysis spp. in relation to population density and environmental conditions on the Swedish west coast. *Harmful Algae* **6**, 218–231 (2007).
45. Sverdrup, H. U. On conditions for the vernal blooming of phytoplankton. *ICES J. Mar. Sci.***18**, 287–295 (1953).
46. Silva, E. et al. Twenty-one years of phytoplankton bloom phenology in the Barents, Norwegian, and North Seas. *Front. Mar. Sci.* **8**, 1–16 (2021).
47. Anderson, D. M. et al. The globally distributed genus Alexandrium: multifaceted roles in marine ecosystems and impacts on human health. *Harmful Algae* **14**, 10–35 (2012).
48. Brosnahan, M. L., Fischer, A. D., Lopez, C. B., Moore, S. K. & Anderson, D. M. Cyst-forming dinoflagellates in a warming climate. *Harmful Algae* **91**, 101728 (2020).
49. Anderson, D. M. & Rengefors, K. Community assembly and seasonal succession of marine dinoflagellates in a temperate estuary: the importance of life cycle events. *Limnol. Oceanogr.* **51**, 860–873 (2006).
50. Jacobs, J., Moore, S. K., Kunkel, K. E. & Sun, L. A framework for examining climate-driven changes to the seasonality and geographical range of coastal pathogens and harmful algae. *Clim. Risk Manag.* **8**, 16–27 (2015).
51. Kirst, G. O. Salinity tolerance of eukaryotic marine algae. *Annu. Rev. Plant Physiol. Plant Mol. Biol.* **41**, 21–53 (1990).
52. Trenberth, K. E. Changes in precipitation with climate change. *Clim. Res.* **47**, 123–138 (2011).
53. Beldring, S., Engen-Skaugen, T., Førland, E. J. & Roald, L. A. Climate change impacts on hydrological processes in Norway based on two methods for transferring regional climate model results to meteorological station sites. *Tellus A Dyn. Meteorol. Oceanogr.* **60**, 439 (2008).
54. McCrystall, M. R., Stroeve, J., Serreze, M., Forbes, B. C. & Screen, J. A. New climate models reveal faster and larger increases in Arctic precipitation than previously projected. *Nat. Commun.* **12**, 6765 (2021).
55. Good, S. et al. The current configuration of the OSTIA system for operational production of foundation sea surface temperature and ice concentration analyses. Remote Sens. **12**, 72 (2020).
56. Merchant, C. J. et al. Satellite-based time-series of sea-surface temperature since 1981 for climate applications. *Sci. Data* **6**, 1–18 (2019).
57. Sakov, P. et al. TOPAZ4: an ocean-sea ice data assimilation system for the North Atlantic and Arctic. *Ocean Sci.* **8**, 633–656 (2012).
58. Xie, J., Bertino, L., Counillon, F., Lisæter, K. A. & Sakov, P. Quality assessment of the TOPAZ4 reanalysis in the Arctic over the period 1991–2013. *Ocean Sci.* **13**, 123–144 (2017).
59. Frouin, R., Franz, B. & Wang, M. Algorithm to estimate PAR from SeaWiFS data Version 1.2-Documentation. *NASA Tech. Memo* **206892**, 46–50 (2003).
60. Craigmile, P. F. & Guttorp, P. Comparing CMIP6 climate model simulations of annual global mean temperatures to a new combined data product. *Earth Space Sci.* **10**, 2468 (2023).
61. Maraun, D. Bias correcting climate change simulations - a critical review. *Curr. Clim. Change Rep.* **2**, 211–220 (2016).
62. Sandø, A. B. et al. Barents Sea plankton production and controlling factors in a fluctuating climate. *ICES J. Mar. Sci.* **78**, 1999–2016 (2021).
63. Semmler, T. et al. AWI AWI-CM1.1MR model output prepared for CMIP6 CMIP. Version 20181218. https://doi.org/10.22033/ESGF/CMIP6.359 (2018).
64. von Storch, J.-S. et al. MPI-M MPIESM1.2-HR model output prepared for CMIP6 HighResMIP. Version 20190721. *Earth Syst. Grid Feder.* https://doi.org/10.22033/ESGF/CMIP6.762 (2017).
65. Bentsen, M. et al. NorESM2-MM model output prepared for CMIP6 CMIP. Version 20230701. *Earth Syst. Grid Feder.* https://doi.org/10.22033/ESGF/CMIP6.506 (2019).

Acknowledgements

ES was funded by the Bjerknes Centre for Climate Research (BCCR) – Centre of Climate Dynamics (SKD) Strategic Project NorHAB-ML and by the institute research fellowship (INSTSTIP) funded by the basic institutional funding through the Norwegian Research Council (#318085). FC was funded by the Trond Mohn Foundation under project number: BFS2018TMT01 and the NFR Climate Futures (309562). LHP has support from the Nansen Centre institutional basic funding (RCN contract 342623). ES and LHP have received funding from the European Space Agency (ESA) Blue Economy

project Earth observations for sustainable aquaculture (4000146872/24/IEF). This work has also received a storage Grant (NORSTORE, NS9039K).

Author contributions

E.S.: Conceptualisation, Data curation, formal analysis, investigation, methodology, visualisation, writing original draft, review and editing. F.C.: Conceptualisation, formal analysis, investigation, methodology, visualisation, review and editing. J.B.: Conceptualisation, formal analysis, investigation, review, and editing. R.D.: Data curation, formal analysis, investigation, methodology, review and editing. S.O.: Formal analysis, investigation, methodology, review and editing. L.H.P.: Formal analysis, investigation, review and editing. N.K.: Formal analysis, investigation, visualisation, review and editing.

Competing interests

The authors declare no competing interests.

Additional information

Supplementary information The online version contains supplementary material available at https://doi.org/10.1038/s43247-025-02421-y.

Correspondence and requests for materials should be addressed to Edson Silva.

Peer review information *Communications Earth & Environment* thanks M.N. and the other, anonymous, reviewer(s) for their contribution to the peer review of this work. Primary handling editors: S.J. and A.D. A peer review file is available.